Solid Freeform Fabrication 2016: Proceedings of the 27th Annual International
Solid Freeform Fabrication Symposium – An Additive Manufacturing Conference
Reviewed Paper

FATIGUE BEHAVIOR AND FAILURE MECHANISMS OF DIRECT LASER DEPOSITED INCONEL 718

Alexander S. Johnson[1], Shao Shuai[1], Nima Shamsaei[2,*], Scott M. Thompson[2], Linkan Bian[3]

[1]Center for Advanced Vehicular Systems (CAVS), Mississippi State University, MS 39762

[2]Department of Mechanical Engineering, Auburn University, Auburn, AL 36849

[3]Department of Industrial and Systems Engineering, Mississippi State University, MS 39762

*Corresponding author: shamsaei@auburn.edu

Abstract

Inconel 718 is considered as a superalloy with a series of superior properties such as high strength, creep-resistance, and corrosion-resistance. Additive manufacturing (AM) is particularly appealing to Inconel 718 because of its near-net-shape production capability to deal with the poor machinability of the alloy. However, AM parts are prone to porosity which is detrimental to the alloy's fatigue properties. As such, further understanding of the fatigue behavior of AM Inconel 718 is much needed. The room temperature fatigue behavior of AM Inconel 718 produced by an Optomec Laser Engineered Net Shaping (LENS^{TM}) system is investigated in this study. Build conditions are carefully controlled to minimize the scatter in fatigue data. The specimens are tested after being subject to a standard heat treatment. Fully reversed strain controlled fatigue tests are performed on round specimens with straight gage section at strain ranges of 0.1% to 1%. Fracture surfaces of fatigue specimens are inspected using a scanning electron microscope. Results are compared to literature for both AM and wrought materials.

Keywords: Fatigue; Failure Mechanisms; Tensile Behavior; Microstructure; Additive Manufacturing; Superalloys

1. Introduction

Inconel 718 is a precipitation hardened nickel-based super alloy used mainly in extreme temperature aerospace applications, such as for turbine blades in jet engines, liquid-fueled rocket components, and cryogenic containers [1]. Inconel alloys are well known for their toughness and difficulty to machine [1]. To circumvent a large portion of the traditional machining time, additive manufacturing (AM) can be used to produce near net-shape parts with only light machining necessary to produce the final product. In general, Fatigue accounts for ~90% of material failures, however, to date, most fatigue research on Inconel 718 has centered on traditionally manufactured Inconel specimens [2-9]. In general, it has been found that fatigue behavior of wrought Inconel 718 begins with a short period of cyclic hardening followed by cyclic softening for the remainder of its fatigue life [6]. In both the low-cycle and high-cycle fatigue regimes, cracks typically initiate

from the surface of specimens and grow to fracture [2, 8]. Most crack growth has been found to be of a transgranular, faceted mode [2-5, 9].

Strain controlled fatigue data is important in that they can provide insights into both the elastic and plastic material behavior during fatigue loading [10]. Very little strain controlled data has been published for wrought Inconel 718 [9], with no strain controlled fatigue data available for AM Inconel 718 to the authors' best knowledge. It is of interest to assess the applicability of AM methods to Inconel 718 and compare its fatigue performance to its traditionally manufactured form. If the performance of the AM material is comparable to wrought, then AM can more justifiably be used to quickly replace broken parts, or more easily manufacture Inconel 718 parts in industry. In this study, Laser Engineered Net Shaping^{TM} (LENS), a blown-powder/laser-based Directed Energy Deposition AM method, is employed for generating Inconel 718 fatigue specimens. Specimens are tested using strain control in order to investigate the fatigue behavior of AM Inconel 718 in both short and long life regimes. The effects of the heat treatment procedure on the microstructure of the material is examined. The strain-life data is compared with the wrought material under the same heat treatment conditions. The specimen fracture surfaces are inspected to understand fatigue crack initiation and propagation characteristics and to compare to reported results in the literature.

2. Experimental Procedure

During the LENS process, multiple nozzles are used to inject powder metal into a central laser beam creating a melt pool on a substrate of similar material to the powder atop a CNC stage. The stage is then moved in the x/y plane (horizontal) relative to the laser beam, in a user-defined path, in order to deposit a line of molten metal. The planar sum of these lines, or tracks, form layers while multiple, stacked layers then form a three dimensional (3D) part that is based on a user-supplied 3D CAD model. During this process, inert gas is pumped into the process chamber to reduce material oxidization.

An argon-purged OPTOMEC LENS^{TM} 750 system equipped with a 1 kW Nd:YAG laser is employed for specimens fabrication. In order to ensure dense, near net-shape parts, a series of preliminary line tests are performed to best determine an operable set of process parameters, i.e.: laser output power, scanning speed and powder flow rate. Using various scan speeds, six lines of arbitrary length are deposited adjacently at different combinations of powder flow rates and laser powers. These deposited lines are cut from the substrate and subsequently sectioned to inspect their cross-sectional shape and fusion with the substrate. Using satisfactory process parameters, 21 cylindrical rods were manufactured using a method consisting of a circular contour deposit with slightly overlapping linear deposits used inside the contour to create the interior of each layer. The direction of the linear deposits are rotated 90 degrees in the x/y plane every layer. Parameters are kept constant throughout the build process. All specimens were printed on the same wrought Inconel 718 substrate spaced approximately 75 mm apart. Previous builds were allowed to cool for several minutes before the next build is started. Specimens were removed from the plate with a hacksaw.

All of the builds were machined into round tensile and fatigue specimens according to ASTM Standard E606 [11] for testing, except one which remained un-machined for inspection of its as-built microstructure. Specimens' geometry is shown in Fig. 1. Fatigue tests were conducted at room temperature in ambient lab atmosphere. All specimens were subject to the standard heat treatment for Inconel 718; 940°C for two hours followed by out-of-furnace air cooling, aging at 718°C for eight hours followed by cooling at a rate of 56°C/hr to 621°C and held for another eight hours followed by air cooling [9].

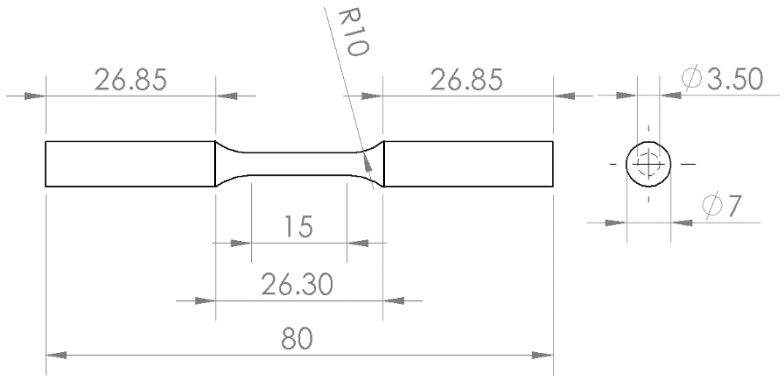

Figure 1. Additive manufactured Inconel 718 fatigue specimens per ASTM E606 [11] (dimensions in mm).

Both a heat treated and as-built specimens were each sectioned, mounted, and polished for microstructure analysis. Etching was accomplished using Waterless Kalling's etchant. Three specimens were monotonically tested to obtain tensile properties of the material. Fully reversed fatigue tests were run on a MTS Landmark system under strain controlled condition at fully reversed strain amplitudes ranging from 0.1% to 1% with at least two tests at most strain levels. Before testing, the gage sections of all specimens were polished to a mirror finish along the loading direction to remove circumferential surface machining marks. After a number of cycles, some tests at high cycle regime were switched to load control for the remainder of their fatigue lives as was also done in the work of Brinkman and Korth [9]. After failure, fracture surfaces were cut from the fatigue specimens and examined via scanning electron microscopy (SEM).

3. Experimental Results

Mechanical properties of the heat treated AM specimens measured in this study and reported elsewhere in the literature, as determined through monotonic testing, are provided in Table 1. If multiple tests of the same type were performed, values were averaged. The tensile mechanical properties of the investigated AM specimens demonstrate to have similar yield stresses (standard deviation of 4.2%), ultimate tensile stresses (UTS) (standard deviation of 1.4%), and elongation to failure (standard deviation of 2.3%) Compared to the wrought Inconel 718 data presented in Table 1, the AM Inconel in this study has slightly lower yield stress and higher UTS.

Table 1. Tensile Properties of Heat Treated Inconel 718.

	0.2% Yield Stress (MPa)	UTS (MPa)	Elongation (%)
This study	895	1514	19.7
Blackwell [12]	1257	1436	13.0
Zhao et al. [13]	1133	1240	9.0
Amsterdam & Kool [14]	891	1213	10.4
Wrought [12, 13]	1113	1353	16.0

Microstructure of the as-built specimen and a specimen after heat treatment are presented in Fig. 2. Builds are sectioned into segments consisting of the grip section and gage section. These sections are cut in half longitudinally (Sections B and C) to view the inner sections of the build. For the heat treated sections, a circular cross section of the grip section is also examined (Section: A). Microstructure is revealed using Waterless Kalling's solution.

Lack of fusion between layers is prevalent in the first several layers deposited near the substrate (Fig. 2(a)). However, these type of defects become nearly non-existent, with only general spherical porosity present in layers further from the substrate (Fig. 2(b)), i.e. in the gage section of specimens. The lack of fusion is confined to the observed grip sections of the selected specimens. Microstructures of specimen regions located near the substrate are found to be mainly comprised of a dendritic structure even after heat treatment (Fig. 2(c)). Further from the substrate after heat treatment, the dendritic structure is found to have mostly dissolved into the general grain structure, though there are residual laves and δ particles present from the dendritic structure (Fig. 2(d), circled) as discussed by Qi et al [15]. Small portions of the dendritic structures remained in the gage section after heat treatment (Fig. 2(e), circled). Average grain size of the heat treated gage section is found to be 43 μm. Figure 2(f) shows the microstructure of the gage section of the as-built specimen. In comparison to the microstructure seen in Fig. 2(e), the grains are found to be much larger and elongated (average of ~170 μm in size along the elongated direction), with more variation in grain size with faint dendritic structure within the grains. Based on microstructural observations, it is clear that the employed heat treatment created more similarly sized grains as well as made them smaller.

Fatigue data, as well as the Coffin-Manson curve fit, are provided in a strain versus life plot, as shown in Fig. 3. It may be seen that the collected data follows a smooth, consistent curve with little scatter. Equation (1) details the specifics of the Coffin-Manson fit for the elastic and plastic portions of the AM Inconel 718 fatigue-life curve [16], i.e.:

$$\frac{\Delta\varepsilon}{2} = \frac{\sigma_{\mathrm{f}}'}{E}(2N_{\mathrm{f}})^{b} + \varepsilon_{\mathrm{f}}'(2N_{\mathrm{f}})^{c} \tag{1}$$

In Eq. (1), $\frac{\Delta\varepsilon}{2}$ is the total strain amplitude, σ_{f}' is the fatigue strength coefficient, E is the modulus of elasticity, $2N_{\mathrm{f}}$ is the reversals to failure, b is the fatigue strength exponent, $\varepsilon_{\mathrm{f}}'$ is the fatigue ductility coefficient, and c is the fatigue ductility exponent. The term $\frac{\sigma_{\mathrm{f}}'}{E}(2N_{\mathrm{f}})^{b}$ expresses

the elastic portion of the curve and the term $\varepsilon_f'(2N_f)^c$ expresses the plastic portion. Equation (2) gives the Coffin-Manson equation fit for the data gathered in this study.

$$\frac{\Delta\varepsilon}{2} = 0.0119(2N_f)^{-0.122} + 2.36(2N_f)^{-0.806} \quad (2)$$

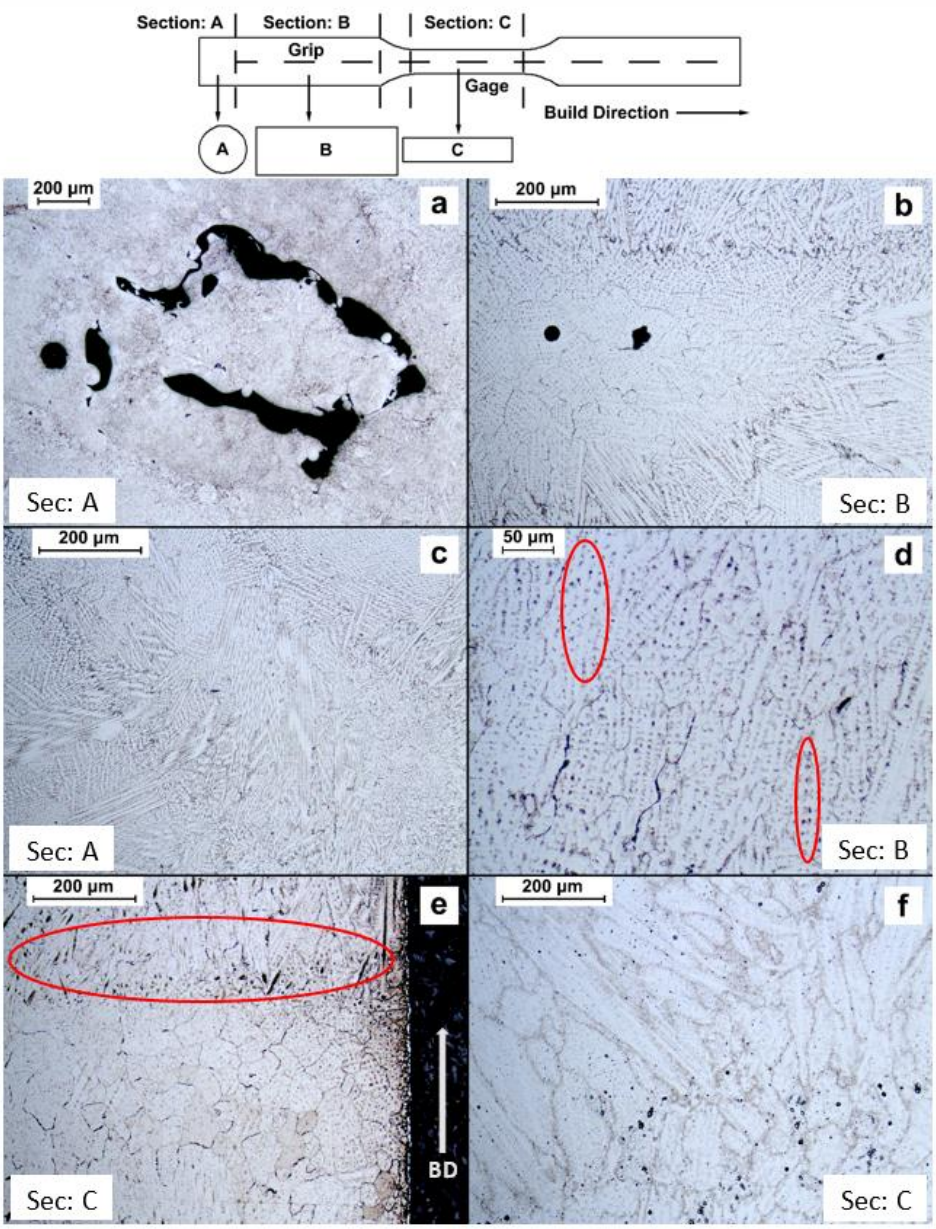

Figure 2. Sectioning diagram and microstructure of heat treated and as-built AM Inconel 718 specimens. (a) Circular cross-section of heat treated grip section (Section: A). (b) Heat treated specimen grip section (Section: B). (c) Residual dendritic structure in heat treated specimen (Section: A). (d) Microstructure of heat treated grip section. (e) Microstructure of heat treated gage section near the surface. (f) Microstructure of as-built gage section. Build direction of (a) and (c) are out of the page. Build direction for (b), (d), (e), and (f) is indicated in (e) (toward the top of the page).

The fatigue lives of the AM Inconel 718 specimens are shorter than those of the wrought Inconel 718 comparison. For comparable strain amplitudes, the fatigue lives of the wrought material were two to three times as long as the AM specimens.

To more directly compare experimental results herein to those of Amsterdam and Kool [14], whom used a different loading ratio during their fatigue testing, the stress values based on each strain interval are determined using measured forces and gage section cross-sectional area. The *R*-value for the data herein is calculated for each specimen and averaged for all tests. An equivalent stress versus life plot is generated and the Smith-Watson-Topper mean stress correction is employed, as shown in Eq. (3) [17], i.e.:

$$\sigma_{\text{eq}} = \sigma_{\text{max}} \sqrt{\frac{1-R}{2}} \tag{3}$$

where σ_{eq} is the equivalent stress amplitude for a test in fully reversed conditions, σ_{max} is the maximum stress for the test data being normalized, and R is the load ratio for the test being normalized. The data correlates very well between this study and the work of Amsterdam and Kool, as shown in Fig. 4.

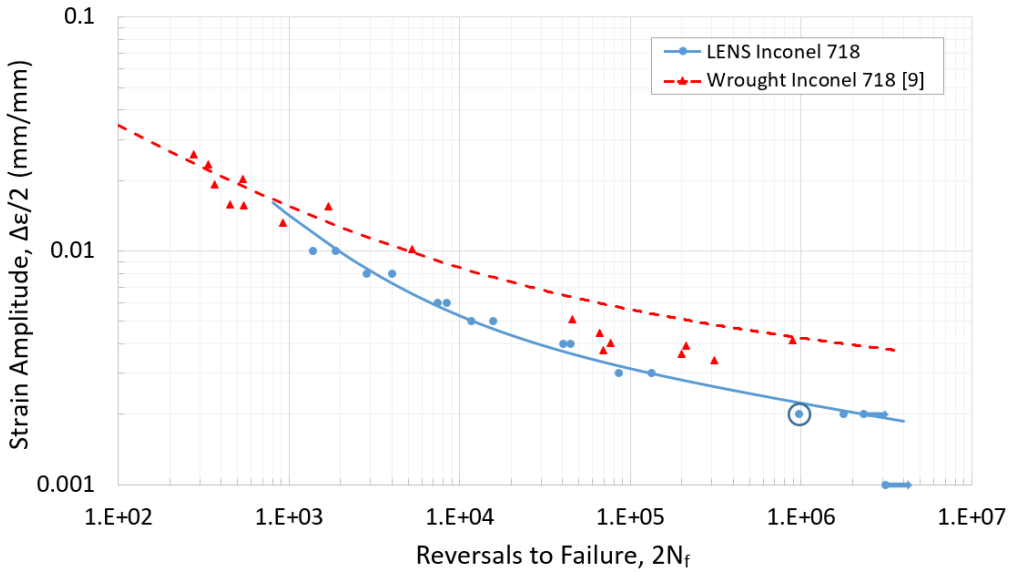

Figure 3. Strain-life fatigue behavior of AM Inconel 718 and its comparison to wrought Inconel 718 [9]. Arrows indicate runout specimens, and the circled point is a specimen that failed much earlier than expected.

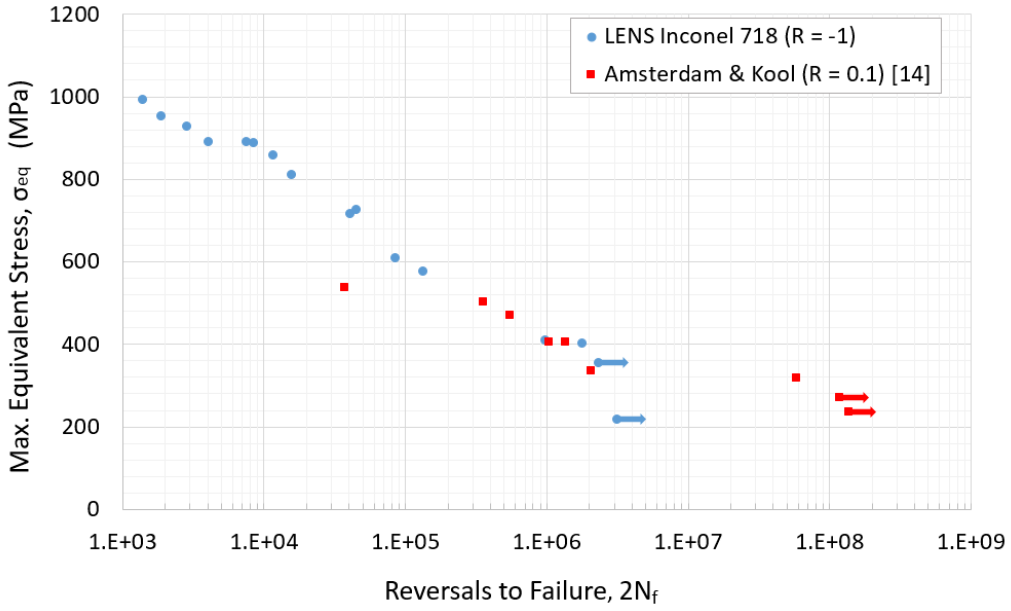

Figure 4. Comparison of normalized R-value stress-life fatigue data of AM Inconel 718 generated in this study with literature [14].

Examples of fracture surfaces obtained from fatigue tests in high and low cycle regimes are presented in Figs. 5 and 6, respectively. All specimens exhibited a distinct crack growth regions (Fig. 5(a) and (c), left side of the red dashed line) and final fracture regions (Fig. 5(a) and (c), right side of the dashed line). Crack growth regions are characterized by fine striations (circled in Fig. 5(b)) running perpendicular to the crack growth direction (white dashed arrows in Figs. 5 and 6). A magnified view of the boundary between the regions on the corresponding surface to Fig. 5(a) is provided in Fig. 5(c). Note that in Fig. 5(c), the parallel line features on the upper right quadrant are part of the final fracture region and are aligned dimples instead of striations. The final fracture regions are distinguished by the high amount of dimpling on the fracture surface (Fig. 5(c), right side of the line), indicating the final fracture is ductile in nature. Most of the crack growth regions are generally flat and of transgranular mode with clear river marks running back towards the initiation point (Fig. 5(d), red solid arrows).

In the specimens shown in Figs. 5 and 6, striations are present on flatter cleavage surfaces as circled in Fig. 5(b) and boxed in Fig. 6(b). Many exposed pores can be seen on the high cycle and low cycle fatigue fracture surface in Fig. 5(d) and Fig. 6(d) respectively, as marked by red solid arrows. Pores this close to the fracture surface likely played a role in reducing the initiation and early growth of fatigue cracks. The fracture surface examined in Figs. 5(e) and 5(f) belong to the specimen from the circled data point in Fig. 3. This sample failed much earlier than other specimens at a strain amplitude of 0.2%. The lower fatigue life likely stems from initiation point in Fig 5(f) (indicated by the arrow), a pore exposed to the specimen surface.

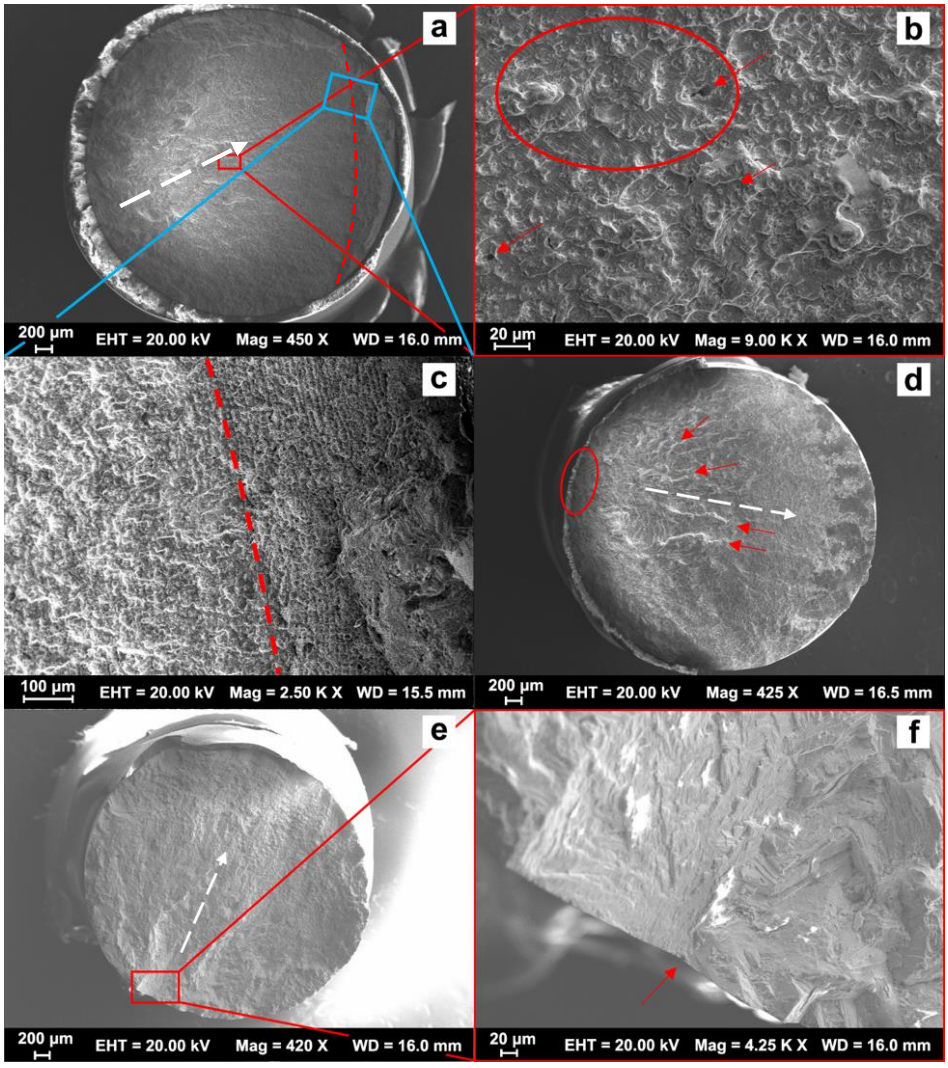

Figure 5. Fatigue fracture surfaces of AM Inconel 718 from high-cycle fatigue tests. Crack propagation directions marked by white dashed arrows. (a) & (b) 0.3% strain amplitude test with notable striations present in (b) (in circled area), exposed pores indicated by red solid arrows. (c) Transition from crack growth to final fracture (indicated by dashed arc). (d) River marks (indicated by red solid arrows) leading back towards initiation site (circled). (e) & (f) 0.2% strain amplitude test that failed earlier than other tests. Crack initiation point is indicated by red solid arrow in (f).

4. Discussion

The mechanical properties of investigated LENS Inconel 718 are similar to AM and wrought reported in the literature. Other data on LENS-type AM Inconel 718 comes from Blackwell [12] and Zhao et al. [13] is presented in Table 1 for comparison. With the full heat treatment data presented by Blackwell, the UTS of the specimens manufactured in this study are similar, within 100 MPa of the average of the three specimens tested. However, the yield and elongation to failure differed by a greater degree. The yield stress reported by Blackwell was significantly greater than the specimens produced in this study. The elongation, on the other hand, was smaller in Blackwell's report by an average of over 6% [12].

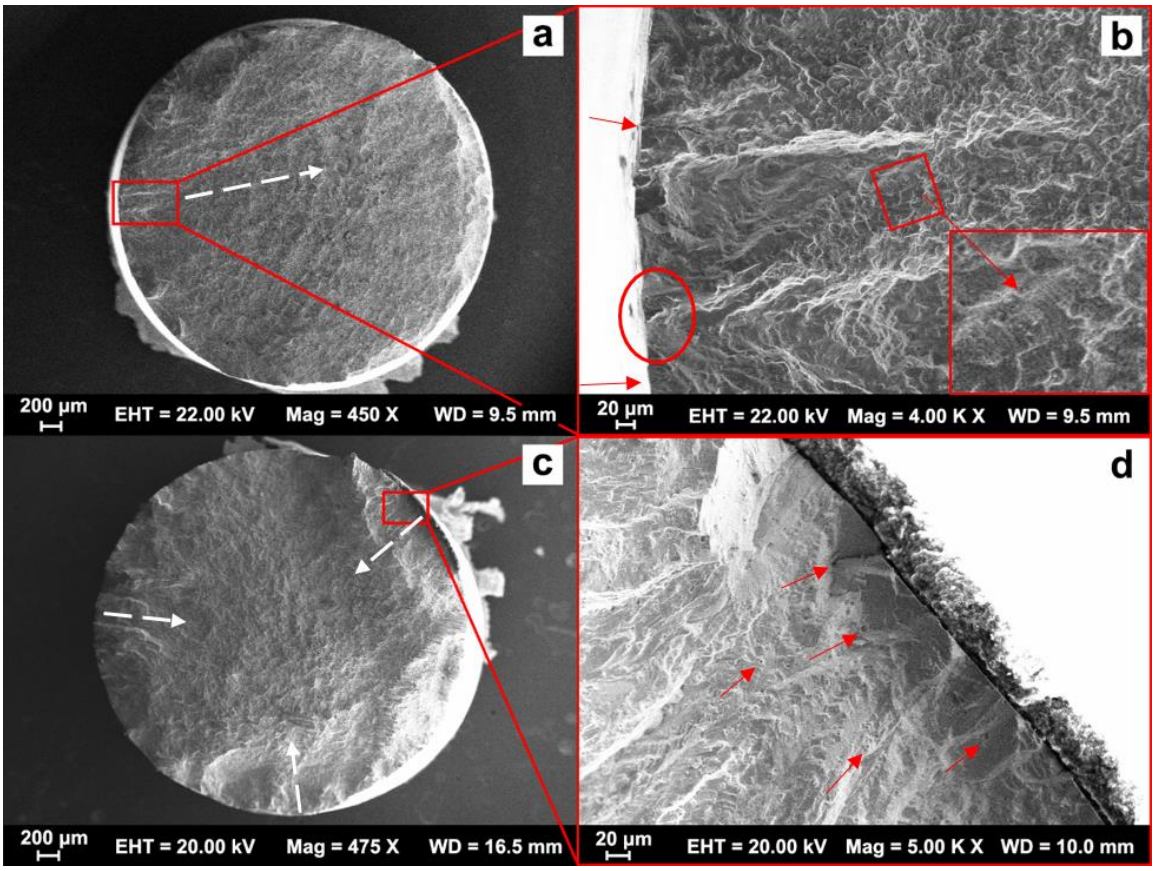

Figure 6. Fatigue fracture surfaces of AM Inconel 718 from low-cycle fatigue tests. Crack propagation directions marked by white dashed arrows. (a) & (b) 1% strain amplitude test, (b) Initiation of the crack (circled), cracks forming from the surface (indicated by red solid arrows). Striations near initiation region (boxed). (c) & (d) 0.6% strain amplitude test, (d) Crack initiation region. Many exposed pores in the crack initiation region (several pores indicated by red solid arrows).

For the data presented in the work of Zhao et al., the same relationship exists with the yield stresses in this study as it has with Blackwell's data. The yield in the current study is lower to about the same degree, though the UTS and the elongation to failure also differ to a greater degree than seen in Blackwell. The specimens produced in this study are much more ductile as compared to Zhao et al. [13], with elongations to failure of 10% more and with an average UTS of 250 MPa more. It is possible that differences in the heat treatment process, such as the addition of hot isostatic pressing (HIPing) in Zhao et al. [13], were responsible for the differences in material behavior. An average of the mechanical properties presented by Amsterdam and Kool [14] had nearly the same yield stress as the material investigated in this study. The average UTS and elongation to failure presented by Amsterdam and Kool were comparable to Zhao et al., and thus, have the same relationship to this study. As compared to averaged wrought Inconel 718 data assembled from Zhao et al. and Blackwell's works, the mechanical properties of the specimens used in the current study have higher UTS and lower yield stress, though it has more comparable elongation to failure [12, 13].

Microstructural comparisons can be easily made with the abundance of literature on the microstructure of AM Inconel 718. Blackwell [12], Zhao et al. [13], Qi et al. [15], and Liu et al. [19] all report on the heat treated and as-built microstructure with Chen et al. [18] reporting solely on as-built. The most common microstructural feature seen in this work, as well as reported in the literature is the significant presence of dendritic microstructure prior to heat treatment in AM Inconel 718 growing approximately in the build direction, as can be seen in the upper region of Fig. 2(b). The long, thin dendrite structures are most likely caused by a high cooling rate during the solidification of the deposited material [12, 13, 18, 19]. After heat treatment, most of the large, elongated grains present in the as-built specimen (Fig. 2(f)) form smaller and more equiaxed grains (Fig. 2(e)). These results are consistent with the results of Zhao et al. [13] and Liu et al. [19]. An interesting phenomenon is presented in Fig. 2(d), which is explained in the research presented by Qi et al. [15] in more detail. The spotted pattern observed (Fig. 2(d), circled) in the microstructure after heat treatment are residual laves and δ phases left over from the dendritic structure present in the as-built material. The solution annealing temperature was not high enough to fully dissolve these phases back into the material matrix [15].

Lack of fusion between the substrate and early deposited layers is also a problem that occurred in the "cross-bonded" specimens presented in Blackwell's work [12]. In this study, lack of fusion in the first several layers of builds near the substrate was also present. These defects are most likely due to rapid cooling and instability of the melt pool as the non-preheated substrate absorbs and disperses directed energy during early layer deposits. As the build gets further away from the substrate, the previously-deposited layers retain more heat and allow for better fusion of subsequent layers. Further investigation with a heated substrate would have to be performed to extrapolate on this build behavior. As large amounts of porosity and lack of fusion tend to occur in the layers near the base of the build (Fig. 2(a)), it is recommended that critical structural portions of builds be built in layers further away from the substrate. Pores found in the gage section of the heat treated specimens are generally circular in shape and did not exceed 45 μm in diameter. This diameter is within the range of pore sizes, 25 and 70 μm, observed by Zhao et al. [13].

The fatigue performance of investigated specimens has been found to be comparable to the AM Inconel 718 performance reported elsewhere [14], as seen in Fig. 4, and less than that of wrought material [9], as seen in Fig. 3. The maximum stress-life fatigue data of AM Inconel 718 presented by Amsterdam and Kool [14] with R = 0.1 has been normalized to equivalent stress-life data using the Smith-Watson-Topper method detailed in Equation (2) and compared to this study in Fig. 4. Heat treatment for the material tested by Amsterdam and Kool was similar to the treatment used in this study with the exception of a higher annealing temperature and different aging times, however, the overall heat treatment time remained the same. Excluding a couple of outliers and the run-out tests for both data sets, this method equates the data nearly exactly, with the bulk of data lying in line with the data presented herein. The fatigue data for wrought Inconel 718 reported by Brinkman and Korth [9] is compared with the current study results in Fig. 3. Note that the heat treatment process used in both studies were the same. While fatigue lives are comparable in short life regime, fatigue lives of LENS Inconel 718 are at least an order of

magnitude shorter than the ones of the wrought counterpart. Porosity present in the AM specimens is the main source of the discrepancy between the wrought and additive material behavior as they serve as crack initiation sites and speed up the fatigue process.

Although the exact point of crack initiation could not be located for a few of the fracture surfaces, indications of fatigue crack initiation from pores, as well as the pores accelerating the fatigue growth could be found in other specimens. For instance, there are unmelted particles near the surface that have initiated the crack (Fig. 6(b)) in several specimens. The fracture surface presented in Fig. 5(e) and 5(f) comes from a 0.2% strain amplitude specimen (Fig. 3, circled) that failed much earlier in its fatigue life than others of the same strain amplitude. There appears to be a pore exposed to the surface of the part that initiated failure and this may explain the much shorter fatigue life. A few of the surfaces also had pores very close to the surface that have initiated fracture like those seen in the initiation region of Fig. 6(c) magnified in Fig. 6(d) (top arrow). The amount of exposed pores in the area indicates it played some role in the early crack growth. Most of the porosity present on the fracture surfaces near the outer surface of the gage section is less than 5 μm in diameter as seen in Fig. 6(d). Exposed pores are present in many of the fracture surfaces in the crack growth regions (Figs. 5(d), 6(b), and 6(d)).

For fracture surface comparisons, there exists only one study on the fatigue behavior of AM Inconel 718 in published literature to the best of authors' knowledge. The work of Amsterdam and Kool [14] details the fracture surface appearance of AM Inconel 718. The description provided of the fracture behavior of the material matches the behavior observed in this study. Initiation from the surface of the material with final fracture regions indicated by the large amount of dimpling [14]. Similar ductile, dimpled final fracture behavior is demonstrated in wrought Inconel 718 studies performed by Ma et al. [3]. The crack propagation observed in specimens tested in this study are in a transgranular mode. This behavior is backed up by wrought crack growth behavior observed in literature [2-5, 9].

5. Conclusions

The mechanical properties, microstructure, fatigue life, and failure modes of additive manufactured (AM) Inconel 718 alloy has been investigated and the results have been discussed. AM Inconel 718 specimens were fabricated using the Laser Engineered Net Shaping (LENS) technique. All specimens were given a standard heat treatment and tested in the same manner as strain-controlled testing of wrought Inconel 718. Resulting fatigue behavior was compared with literature along with microstructure, mechanical properties, and fracture surfaces. The following conclusions can be drawn from acquired data:

1. As-built AM specimens had elongated grains in the build direction as well as a large amount of dendritic structure. The issue of lack of fusion near the substrate during builds needs to be further explored in an attempt to produce denser builds. Preheating the substrate may alleviate this lack of fusion.

2. Heat treatment of the specimens was found to create smaller and more uniform grain structure. Residual dendrites still existed in some portions of the investigated specimens.

In places where dendrite structures were dissolved, residual laves and δ-phases were found to remain.

3. The mechanical properties of the specimens produced in this study is comparable to those reported in the literature for wrought and other AM Inconel 718 specimens. However, the investigated specimens herein possessed slightly lower yield stress and higher ultimate tensile stress as compared to both wrought and other available data for AM Inconel 718.

4. Cracks were found to originate from the surface, and in some cases, near-surface pores in LENS Inconel 718. Cracks grew in a transgranular mode during propagation. Final fracture occurred in a ductile, dimpled mode.

5. While fatigue lives are comparable in short-life regime, fatigue lives of LENS Inconel 718 are at least an order of magnitude shorter than its wrought counterpart in the long-life regime. To enhance their fatigue resistance, further improvements need to be made to the additive manufacturing, or post-manufacturing processes, in order to more consistently produce parts with less porosity and more uniform microstructure.

Acknowledgments

Research was partially sponsored by the Army Research Laboratory and was accomplished under Cooperative Agreement Number W911NF-15-2-0025. The views and conclusions contained in this document are those of the authors and should not be interpreted as representing the official policies, either expressed or implied, of the Army Research Laboratory or the U.S. Government. The U.S. Government is authorized to reproduce and distribute reprints for Government purposes notwithstanding any copyright notation herein. This manuscript was prepared while Nima Shamsaei and Scott Thompson were Assistant Professors at Mississippi State University.

References

[1] *Inconel Alloy 718*. Publication no. SMC-045. Special Metals, Sept. 2007. Web. <http://www.specialmetals.com/documents/Inconel%20alloy%20718.pdf>.

[2] Chen, Q., N. Kawagoishi, and H. Nisitani. "Evaluation of fatigue crack growth rate and life prediction of Inconel 718 at room and elevated temperatures."*Materials Science and Engineering: A* 277.1 (2000): 250-257.

[3] Ma, Xian-feng, et al. "Fatigue and fracture behavior of nickel-based superalloy Inconel 718 up to the very high cycle regime." *Journal of Zhejiang University Science A* 11.10 (2010): 727-737.

[4] Mercer, C., A. B. O. Soboyejo, and W. O. Soboyejo. "Micromechanisms of fatigue crack growth in a forged Inconel 718 nickel-based superalloy." *Materials Science and Engineering*: A 270.2 (1999): 308-322.

[5] Andersson, Henrik, and Christer Persson. "In-situ SEM study of fatigue crack growth behaviour in IN718." *International Journal of Fatigue* 26.3 (2004): 211-219.

[6] Worthem, D. W., et al. "Inhomogeneous deformation in Inconel 718 during monotonic and cyclic loadings." *Metallurgical Transactions A* 21.12 (1990): 3215-3220.

[7] Mercer, C., A. B. O. Soboyejo, and W. O. Soboyejo. "Micromechanisms of fatigue crack growth in a single crystal Inconel 718 nickel-based superalloy."*Acta materialia* 47.9 (1999): 2727-2740.

[8] Kawagoishi, N., Q. Chen, and H. Nisitani. "Fatigue strength of Inconel 718 at elevated temperatures." *Fatigue and Fracture of Engineering Materials and Structures* 23.3 (2000): 209-216.

[9] Brinkman, C. and GE Korth. "Strain Fatigue and Tensile Behavior of Inconel® 718 from Room Temperature to 650°C." *Journal of Testing and Evaluation*. 2.4 (1974): 249-259.

[10] Roessle, M. L., and A. Fatemi. "Strain-controlled fatigue properties of steels and some simple approximations." *International journal of fatigue* 22.6 (2000): 495-511.

[11] ASTM E606/E606M-12 Standard Test Method for Strain-Controlled Fatigue Testing, ASTM International, West Conshohocken, PA, 2012, http://dx.doi.org/10.1520/E0606_E0606M-12

[12] Blackwell, P. L. "The mechanical and microstructural characteristics of laser-deposited IN718." *Journal of materials processing technology* 170.1 (2005): 240-246.

[13] Zhao, Xiaoming, et al. "Study on microstructure and mechanical properties of laser rapid forming Inconel 718." *Materials Science and Engineering: A* 478.1 (2008): 119-124.

[14] Amsterdam, E., and G. A. Kool. "High cycle fatigue of laser beam deposited Ti-6Al-4V and Inconel 718." *ICAF 2009, Bridging the Gap between Theory and Operational Practice*. Springer Netherlands, 2009. 1261-1274.

[15] Qi, H., M. Azer, and A. Ritter. "Studies of standard heat treatment effects on microstructure and mechanical properties of laser net shape manufactured Inconel 718." *Metallurgical and Materials Transactions A* 40.10 (2009): 2410-2422.

[16] R. I. Stephens, A. Fatemi, R. R. Stephens, and Fuchs, H. O. *Metal Fatigue in Engineering*. New York: Wiley, 2001. Print.

[17] Dowling, N. E. "Mean stress effects in strain–life fatigue." *Fatigue & Fracture of Engineering Materials & Structures* 32.12 (2009): 1004-1019.

[18] Chen, Yuan, et al. "Dendritic microstructure and hot cracking of laser additive manufactured Inconel 718 under improved base cooling." *Journal of Alloys and Compounds* 670 (2016): 312-321.

[19] Liu, Fencheng, et al. "Microstructure and residual stress of laser rapid formed Inconel 718 nickel-base superalloy." *Optics & laser technology* 43.1 (2011): 208-213.